High temperature oxidation of AISI 441 in simulated solid oxide fuel cell anode side conditions

Corrosion Science 203 (2022) 110338

Contents lists available at ScienceDirect

Corrosion Science

journal homepage: www.elsevier.com/locate/corsci

High temperature oxidation of AISI 441 in simulated solid oxide fuel cell anode side conditions

Anton Chyrkin [a], Kerem Ozgur Gunduz [a,b], Vijayshankar Asokan [a], Jan-Erik Svensson [a], Jan Froitzheim [a,*]

[a] Chalmers University of Technology, Department of Chemistry and Chemical Engineering, Division of Energy and Materials, Kemivägen 10, SE-41296 Gothenburg, Sweden

[b] Gebze Technical University, Department of Materials Science and Engineering, 41400 Gebze, Kocaeli, Turkey

ARTICLE INFO

Keywords:
AISI 441
Interconnect
Water vapor
Hydrogen
Solid oxide fuel cells
Anode side

ABSTRACT

This study investigates the corrosion of AISI 441 in simulated anode conditions of solid oxide fuel cells (SOFCs). Several parameters such as temperature, humidity, surface condition, pre-oxidation temperature and environment, were investigated. Samples pre-oxidized at 800 °C were protective at 550–900 °C, while as-received samples showed protective behavior only at 900 °C. Additional exposures performed at 600 °C revealed the negative effect of increasing steam concentration, the beneficial effect of grinding, while pre-oxidation at 600 °C did not improve the protectiveness. The role and the interplay of the aforementioned factors are discussed.

1. Introduction

Solid oxide fuel cells (SOFCs) are devices that convert the chemical energy of a fuel such as hydrogen into electricity through an electrochemical reaction with high efficiency reaching up to 74% [1–4]. SOFCs have many advantages, such as fuel flexibility, mechanical reliability, silent operation, zero particulate emissions, etc. [1–3,5]. However, one cell only produces approximately 1 V according to the Nernst equation [6–8]. Thus, a component called an interconnect must be employed to electrically connect neighboring cells to form a stack in order to obtain sufficient power for most applications [6–9]. In addition to the electrical connection, a corrugated interconnect provides gas channels required for anodic and cathodic reactions. Owing to the development of new electrode and electrolyte materials as well as improved design, SOFCs can now operate at temperatures between 550 and 900 °C [3,5,10]. This decrease in operating temperatures made it possible for the employment of metallic materials as interconnects. The best candidates among metallic materials are Cr_2O_3-forming ferritic stainless steels (FSS) owing to their good thermal expansion coefficient (TEC) compatibility with the other components of the cell, moderate oxidation resistance, relatively low area-specific resistance compared to Al_2O_3 and SiO_2, simple manufacturing, and relatively low cost [6–9]. However, there are several problems associated with the employment of FSS as an interconnect material in SOFCs, such as Cr evaporation [11–13], high area-specific resistance (ASR) [14] and high temperature corrosion [15–17]. Various strategies have been developed against Cr evaporation and high ASR. One approach is the deposition of thin films such as Co and Ce/Co to reduce Cr evaporation rate and Cr_2O_3 growth kinetics, respectively [18–20]. This strategy is also beneficial to reduce the ASR. A particular type of corrosion, the dual-atmosphere effect, occurs when hydrogen is used as a fuel, i.e., hydrogen diffuses in the metal from the fuel to the air side, causing the formation of Fe-rich non-protective oxide on the air side instead of protective Cr_2O_3 [21–23].

However, non-protective oxidation occurs not only on the air side of the interconnect in dual-atmosphere conditions. Fe-rich oxides form on the fuel side as well, which might additionally exacerbate the chemical degradation of the interconnect. In fact, many studies on the oxidation behavior of FSS in Ar-H_2-H_2O and Ar-H_2O atmospheres are available in literature [24–28]. Several hypotheses have been proposed to reveal the mechanism of breakaway corrosion in humid and/or hydrogen-containing environments. Earlier hypotheses were mostly based on altering the oxide scale properties in H_2O-rich environments, neglecting the effect of dissolved H on the transport of species such as Cr and O in the alloy [25,29–31].

However, other authors have demonstrated that, internal oxidation of Cr is favored under Ar-H_2-H_2O and Ar-H_2O [24,26,28,32]. This effect is further intensified when more water vapor is introduced [24,28]. The authors hypothesized that hydrogen dissolved in the Fe-Cr alloy

* Corresponding author.
E-mail address: Jan.froitzheim@chalmers.se (J. Froitzheim).

https://doi.org/10.1016/j.corsci.2022.110338
Received 23 November 2021; Received in revised form 21 April 2022; Accepted 21 April 2022
Available online 25 April 2022

expanded the lattice, which resulted in an enhanced oxygen transport [24,26]. The enhanced oxygen permeability thus favored internal oxidation, preventing the formation of an external protective Cr_2O_3 layer as well as facilitating the formation of Fe-based non-protective oxides. In addition, dual-atmosphere exposures delivered clear experimental evidence of non-protective oxidation behavior of the air side of the FSS under dual-atmosphere conditions [15,17,21–23]. Therefore, both aspects should be investigated to further understand the effect of H and H_2O on the formation of Fe-base oxides under dual (H_2/H_2O vs. Air) and single (H_2/H_2O) fuel conditions relevant for SOFCs.

Young et al. [27] studied the effect of temperature on the oxidation behavior of several non-pre-oxidized FSS, including AISI 441, under single Ar-4%H_2-20%H_2O atmosphere 500–900 °C to simulate the fuel side of the interconnects. The study showed that Fe-rich oxide formation occurred at low temperatures around 600 °C, while above 600 °C, protectiveness was improved and at 800 °C, only external Cr_2O_3 was observed. In that study, Ar-4%H_2-20%H_2O atmosphere was chosen to simulate the anode conditions in an SOFC while suppressing the Cr vaporization as a result of low pO_2. Less humid environments containing e.g., 3% H_2O are also relevant, especially for the stack inlet where water vapor concentration is lower than that of the outlet and deserve attention. In our previous study [33], the effects of temperature and pre-oxidation on the air-side oxidation of AISI 441 steel under dual-atmosphere conditions were investigated. It was hypothesized that dissolved hydrogen decelerates grain boundary diffusion of Cr, resulting in non-protective Fe-rich oxide formation. To gain new insight on the effect of H on the breakdown of Fe-Cr steels, the fuel-side corrosion behavior of AISI 441 steel exposed in Ar-5%H_2-3%H_2O for 336 h between 550 and 900 °C was investigated in the present study. The effects of humidity and surface preparation were also studied at 600 °C where the non-protective behavior is most pronounced.

2. Materials and methods

2.1. Sample preparation

Hot-rolled 0.2 and 0.3 mm thick AISI 441 was used in this study. The chemical compositions of these sheets are given in Table 1.

The sheets were received in bright annealed condition with a surface roughness of 0.1–0.3 μm and average grain size of 29 μm according to ASTM E112 (Heyn intercept method). Two types of samples were prepared for exposure in dual- and single-atmosphere conditions. For dual-atmosphere exposures, circular specimens were obtained by employing a punch with a diameter of 21 mm, while for single atmosphere exposures, sheets were cut into rectangular-shaped samples in the dimensions 20 mm × 10 mm. To reveal the effect of surface condition, samples with two different surface finishes were used in this study i) as-received, and ii) ground. Ground samples were prepared by grinding samples with 320–1200 grit emery papers from 0.3 to 0.2 mm thickness. Therefore, all investigated samples had a thickness of 0.2 mm. Sheet thicknesses of 0.2–0.5 mm are commonly used for interconnect applications [34]. After the surface preparation step, samples were first rinsed with deionized water and cleaned in an ultrasonic bath successively in acetone and ethanol twice for 10 min in each. A Mettler Toledo XP6 microbalance with 1 μg sensitivity was used to weigh the samples before and after pre-oxidation.

2.2. Pre-oxidation

Three different pre-oxidation procedures were followed in this study and with the parameters summarized in Table 2.

The first procedure, called 800Air, was performed in a tube furnace at 800 °C for 20 min under Air+ 3%H_2O atmosphere with a flow rate of 280 sml min^{-1}. Samples were directly inserted into the pre-heated furnace and taken out after 20 min and cooled in laboratory air. The samples were weighed after the pre-oxidation, revealing a mass gain of approximately 0.008 mg/cm^2, which correlates well with the previous studies [17]. The thickness of the oxide scale (50 nm) after 800Air procedure is calculated based on the mass gain. The second procedure, called 600Air, was performed in an identical manner to 800Air but at 600 °C for a duration of 36 h instead of 20 min. The third procedure, called 600H_2, was performed at 600 °C for 10 h in Ar-5%H_2 + 0.3%H_2O. The steel specimens were heated to 600 °C and cooled down with a heating rate of 1 °C min^{-1} in a flow of Ar-5%H_2 + 0.3%H_2O. In order to establish 0.3% humidity, Ar-5%H_2 gas was first bubbled through a round bottom flask at room temperature and then passed through a cooling condenser kept at − 8 °C. The H_2O concentration was controlled by a chilled mirror hygrometer (Michell Optidew Vision) and found as − 8 °C which corresponds to 0.3%H_2O. It should be noted that all humidity concentrations refer to absolute humidity.

The duration of the second and third procedures was chosen to obtain equally thick (50 nm corresponding to 0.008 mg/cm^2 oxygen uptake) pre-oxidation layers on as-received samples in order to compare the protectiveness and oxygen uptake of differently formed pre-oxidation scales.

2.3. Dual-atmosphere exposures

The details of the experimental procedure for the dual-atmosphere exposures can be found elsewhere [15]. The dual-atmosphere exposure parameters performed in this study are summarized in Table 3. The air atmospheres were set as Air+ 3%H_2O.

The first set of exposures investigates the effect of temperature and is performed between 550 and 800 °C in 97%(Ar-5%H_2)+ 3%H_2O, which corresponds to Ar-4.75%H_2-3%H_2O in parallel with Air+ 3%H_2O for 336 h on as-received and 800Air-pre-oxidized samples. Since the hydrogen concentration is almost the same with the dry gas, it is referred in the text as Ar-5%H_2-3%H_2O. The dewpoint of the gas was controlled with a chilled-mirror hygrometer and measured as 24.4 °C. The fuel sides of the samples (exposed to low pO_2) were investigated in this study. As previously reported, the most severe dual-atmosphere effect at the air side was observed at 600 °C [16,33]. Therefore, additional exposures were performed at 600 °C to study the effect of grinding, pre-oxidation parameters, and the effect of humidity. Ground non-pre-oxidized and differently pre-oxidized samples (800Air, 600Air, 600H_2 procedures) were exposed in the same conditions as in the exposures with varying temperature. To study the effect of humidity on the

Table 2
Pre-oxidation procedures performed in this study.

Pre-oxidation	Temperature (°C)	Atmosphere	Duration	Mass gain (mg/cm^2)	pO_2 (bar)
800Air	800	Air + 3%H_2O	20 min	0.008	0.2
600Air	600	Air + 3%H_2O	36 h	0.009	0.2
600H_2	600	Ar-5%H_2 + 0.3%H_2O	11 h	0.009	1.23×10^{-26}

Table 1
Chemical composition of the AISI 441 steel (in wt%).

Material	Fe	Cr	Mn	Si	Ti	Nb	Ni	C	S	P	N
AISI 441/ EN 1.4509	Bal.	17.56	0.35	0.59	0.173	0.39	0.26	0.014	0.001	0.03	0.017

Table 3
Different dual atmosphere exposure conditions used in this study.

Exposure	Temperature (°C)	Atmosphere (Anode side)	Duration	pO_2 (Bar)
Temperature Dependency	550–800	Ar-5%H_2-3% H_2O	336 h	2×10^{-26} (550 °C) 4×10^{-19} (800 °C)
High humidity	600	Ar-4%H_2-20% H_2O	336 h	8.55×10^{-23}
Low Humidity	600	Ar-5%H_2	336 h	1.1×10^{-27}

fuel side, dual-atmosphere exposures were performed for 336 h under simulated fuel conditions with different water vapor concentrations at 600 °C. Either dry Ar-5%H_2 or 80%(Ar-5%H_2)+ 20%H_2O, which corresponds to Ar-4%H_2-20%H_2O, was used on the fuel side, while the air side was exposed to Air + 3%H_2O in both cases. In all dual-atmosphere exposures, the flow rate of the fuel side was 100 sml min^{-1} while the flow on the air side was 8800 sml min^{-1}. The high flow rate on the air side was selected to reach the flow-independent Cr evaporation regime [12]. A chilled mirror-hygrometer was used to control the humidity level on the fuel and air sides. When dry hydrogen was used, the dew point was measured as − 24 °C, which corresponds roughly to 900 ppm water vapor. In order to avoid thermal stresses, a heating/cooling rate of 1 °C min^{-1} was chosen. All exposures were performed at least twice in order to be sure that the results are reproducible.

2.4. Single atmosphere exposures

From the dual-atmosphere exposures, it is not possible to obtain mass gains, since the mass gains on the fuel and air sides are not equal. Furthermore, the interaction of the sample with the gold sealant does not allow for accurate gravimetry. Therefore, to obtain mass gains, single atmosphere exposures in tube furnaces were performed under Ar-5%H_2-3%H_2O between 550 °C–900 °C for 336 h by exposing samples with and without 800Air-pre-oxidation with the same heating/cooling rate. The humidity was controlled by the same chilled mirror hygrometer and the corresponding dew point was found as 24.4 °C. The flow rate in this case was selected as 250 sml min^{-1}. The lowest temperature for single atmosphere exposures was selected as 550 °C as in our previous study the samples were protective at 500 °C [33], while the upper limit was selected as 900 °C to further investigate the effect of temperature on the protectiveness of AISI 441 on the fuel side. The samples were weighed before and after exposures using a Mettler Toledo XP6 microbalance. The mass gain of a pre-oxidized sample refers to the mass gain obtained during the exposure carried out after pre-oxidation.

2.5. Characterizations

After the exposures, cross-sections were prepared using a Leica TIC 3X broad ion beam for SEM-EDX investigations. A FEI ESEM QUANTA 200 equipped with an Oxford X-max 80 EDX detector and a Zeiss LEO Ultra FE-55 equipped with an in-lens detector were used for cross-sectional SEM-EDX investigations. For further investigations of cross-sections, site-specific lift-outs were performed in a FEI Versa 3D focused ion beam/scanning electron microscope (FIB-SEM) equipped with an Oxford Instruments OmniProbe 100 micromanipulator. Analytical scanning transmission electron microscopy (STEM/EDX) analyses were carried out in a FEI Titan 80–300 TEM/STEM equipped with an Oxford Instruments INCA X-sight EDX system.

3. Results

3.1. Effect of temperature on as-received and 800Air-pre-oxidized samples

Fig. 1a shows the fuel side oxide scale thickness values obtained in dual atmosphere exposures performed under Ar-5%H_2-3%H_2O atmosphere between 550 and 800 °C for 336 h on as-received and 800Air-pre-oxidized samples. The as-received samples showed a remarkable improvement in protectiveness over 650 °C resulting in lower oxide scale thickness values. The 800Air-pre-oxidized samples showed a completely protective behavior between 550 and 800 °C after 336 h. Oxide thickness values continuously increased from 550 to 800 °C. At 800 °C, the as-received samples had slightly thicker oxide scales in comparison with the pre-oxidized samples.

To complement the thickness data in Fig. 1a with mass gain data and to expose samples at 900 °C, the experiments were repeated in the same atmosphere in single atmosphere conditions between 550 and 900 °C for 336 h. The obtained mass gain data are presented in Fig. 1b. The remarkable improvement in protectiveness of as-received samples above 650 °C is also reflected in the recorded mass gains. On the as-received samples, at 900 °C, slightly higher mass gains were obtained to 800 °C while at 900 °C both specimens demonstrated almost equal mass gains. This comparison clearly showed that the as-received sample forms a fully protective Cr_2O_3 scale at 900 °C.

An additional comparison between Fig. 1a and b revealed that the thickness and mass gains correlate well between 550 and 800 °C which shows that same trend exist on the fuel side of the dual atmosphere exposures and single fuel exposures as expected.

Fig. 2 shows the SEM cross-sections of as-received samples exposed between 550 and 900 °C for 336 h in Ar-5%H_2-3%H_2O and Fig. 3 shows the SEM-EDX mappings of the same regions. According to Figs. 2 and 3, at 550 and 600 °C, the oxide scales were almost identical and composed of an outward grown porous Fe_3O_4 layer according to SEM-EDX and XRD analysis (not given here). At 550 °C, a continuous internal oxidation zone (IOZ) was present below the outward grown Fe_3O_4 layer. However, at 600 °C, the continuity of the IOZ was interrupted and locally replaced by an inward grown $(Fe,Cr)_3O_4$ phase. According to several studies, the IOZ layer consists of unreacted Fe, Cr_2O_3 and Cr rich (55 at% cation) $(FeCr)_3O_4$ type oxides [15,24,35–37]. At 650 °C (Figs. 2c and 3c), no IOZ was detected in the steel subsurface. Instead, an outward grown oxide layer composed of a lamellar structure and an inward grown, multi-layer oxide subscale consisting of two different layers were observed. In the SEM-EDX analysis, only Fe as a cation is detected in the outward grown part of the oxide layer. The inner part of the oxide scale comprises of an $(Fe,Cr,Mn)_3O_4$ layer (EDX analysis 28.9 at% Fe, 19.8 at% Cr and 0.4 at% Mn) and a Cr-rich sublayer (EDX analysis 32.6 at% Cr, 15 at% Fe and 0.6 at% Mn) next to the metal-oxide interface (Fig. 3c). A detailed TEM-EDX analysis of samples exposed at 650 °C is given in Fig. 4. According to Fig. 4, the lamellae were composed of pure Fe embedded in an Fe_3O_4 matrix. No Cr was detected in the TEM-EDX analysis. The formation of the lamellar structure is the direct result of the eutectoid reaction from FeO into Fe+Fe_3O_4, as previously reported [38–40]. The samples were heated and cooled at 1 °C/min, and thus the slow cooling rate presumably allowed the eutectoid transformation to take place at that temperature. At 700 °C, similarly to 650 °C, the oxide scale consisted of one outward and one inward grown layer (Fig. 3d). The outward grown scale consisted of two different phases. One phase was found as a band just over the original steel surface with a darker contrast as compared to the continuous phase above it. According to the literature, this dark phase (marked Fe_3O_4) is identified as magnetite seam, which nucleates at the FeO/metal interface as a result of the eutectoid transformation [39,40]. No lamellar structure was found on the samples exposed at 700 °C. The magnetite seam and lamellae formation have been discussed in several studies [41–43]. According to the SEM-EDX mapping, the Cr concentration of $(Fe,Cr)_3O_4$ sublayer at 700 °C was

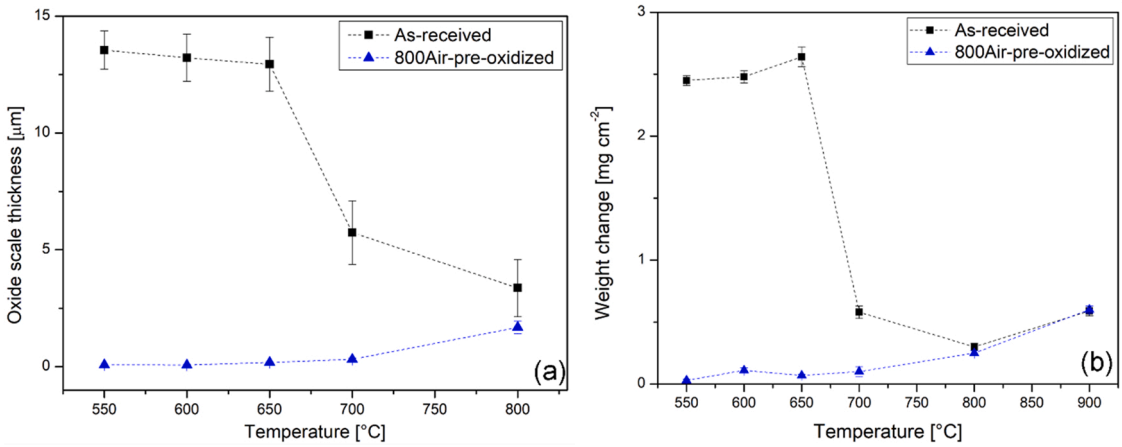

Fig. 1. Oxide scale thickness and mass gains of as-received and 800Air-pre-oxidized samples obtained through single and dual exposures for 336 h. a) Oxide scale thickness values of samples exposed in dual atmosphere exposures between 550 and 800 °C a) Mass gains obtained in single atmosphere (Ar-5%H_2-3%H_2O) between 550 and 900 °C.

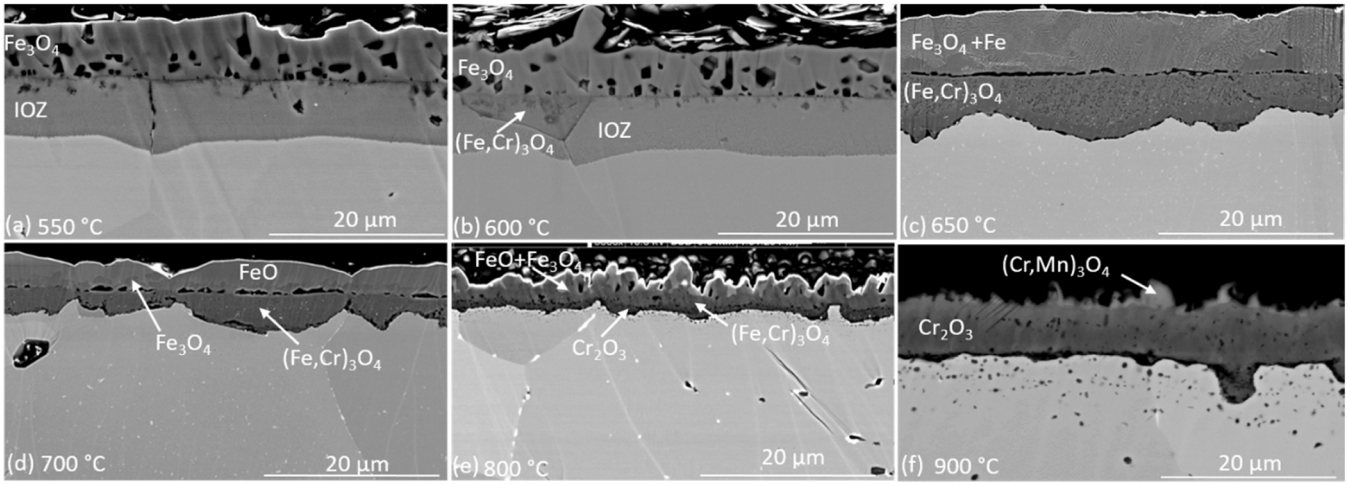

Fig. 2. Cross-sectional SEM images of the oxide scales formed in Ar-5%H_2-3%H_2O at 550–900 °C after 336 h. a) 550 °C, b) 600 °C, c) 650 °C, d) 700 °C, e) 800 °C, f) 900 °C Except 900 °C images were captured from the dual atmosphere exposure samples.

determined as 30.8 with a slight enrichment (32.2 at% Cr) at the metal-oxide interface. At 800 °C, the oxide scale can be separated into three regions, namely: i) the outermost region composed of an undulating gas-scale interface including regions with darker and brighter contrast, ii) the intermediate region between the outermost layer and the pore-band with a dark contrast, and iii) the region below the pore band with a slightly darker contrast than the intermediate layer. According to SEM-EDX mapping, the region below the pore band is rich in Cr_2O_3 (almost 40 at% Cr according to EDX) this matches XRD results (not given here) showing the presence of Cr_2O_3. The region above the pore band corresponds to $(Fe,Cr,Mn)_3O_4$ containing 10.6 at% Fe 30.7 at % Cr, 4.4 at% Mn confirmed by XRD. The outer region is rich in Fe, corresponding to FeO+Fe_3O_4, though in some localized regions Cr was also detected on the outermost region. Since Fe is mostly concentrated on the outermost part of the oxide scale, it is suggested that Fe-rich phases formed during the earlier stages of oxidation. Later on, with the establishment of a passivating Cr_2O_3 layer, these phases transformed gradually into Cr-rich mixed oxides. Additionally, internally oxidized Ti particles were detected in the surface-near region below the oxide scale. No magnetite seam or lamellae were detected at 800 °C. Similar oxide scales were also obtained on AISI 441 FSS exposed at 800 °C in H_2/H_2O mixtures by Ardigo et al. [44]. At 900 °C, a typical protective double-layered oxide scale, composed of a $(Cr,Mn)_3O_4$ cap layer on a Cr_2O_3 layer, was obtained. However, at the gas-oxide scale interface, Mn-rich whiskers can be seen. Internally oxidized Ti was also present below the oxide scale. Clearly, increasing the temperature enhances the protectiveness of the oxide scales on as-received samples, especially above 800 °C.

Fig. 5 depicts the fuel-side SEM cross-sections of 800Air-pre-oxidized samples exposed in dual conditions between 550 and 800 °C for 336 h including the SEM-EDX mapping of 800 °C. In addition, SEM cross-sections and SEM-EDX mapping of 800Air-pre-oxidized samples oxidized in single atmosphere conditions at 900 °C were also included in Fig. 5. According to the SEM images, the specimens pre-oxidized in these conditions exhibited consistently protective behavior within the selected temperature range after 336 h. Oxide scales were composed of typical duplex scales consisting of $(Cr,Mn)_3O_4$ and Cr_2O_3. From 550–900 °C, a gradual increase in oxide scale thickness was observed owing to the acceleration in Cr_2O_3 growth rate with increasing temperature.

3.2. *Effect of humidity*

Fig. 6 presents SEM images of cross-sections of the fuel side of as-received and 800Air-pre-oxidized samples exposed in dual conditions with different simulated fuels (dry Ar-5%H_2, Ar-5%H_2-3%H_2O and Ar-

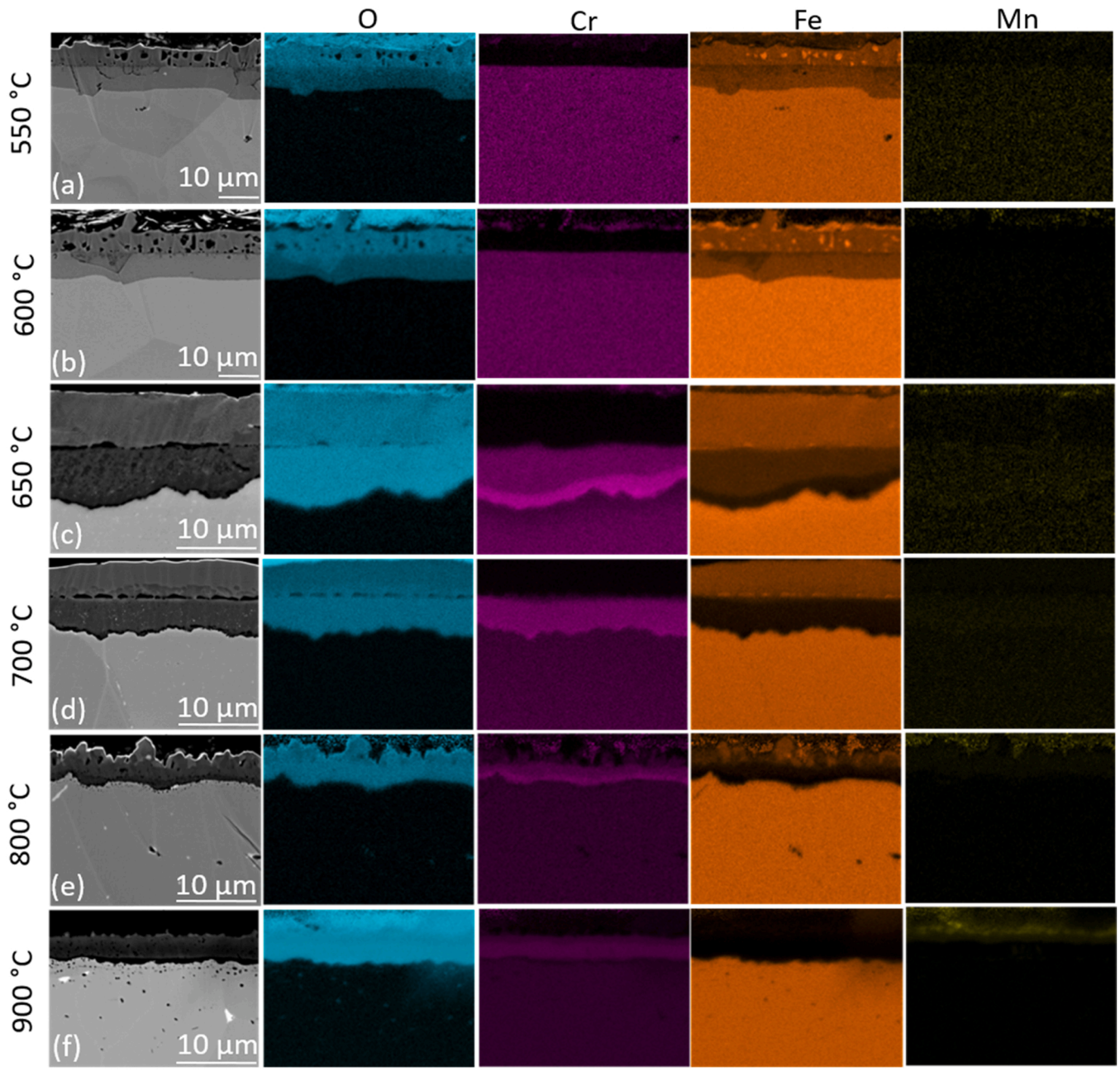

Fig. 3. Fuel side cross-section SEM-EDX mapping of as-received samples exposed in Ar-5%H_2-3%H_2O after 336 h. a) 550 °C, b) 600 °C, c) 650 °C, d) 700 °C, e) 800 °C, f) 900 °C. Except 900 °C analysis was performed on the dual atmosphere exposure samples and please note the different magnifications.

4%H_2-20%H_2O) at 600 °C for 336 h. Dry Ar-5% H_2 contained approximately 900 ppm H_2O according to dew point measurements. The obtained results showed that the as-received samples exhibited a protective scale only in dry conditions while Fe-rich non-protective oxides formed in 3% and 20% humidity-containing gases. A comparison between 3% and 20% humidity showed that corrosion was more severe for higher H_2O content. Furthermore, 800Air-pre-oxidized samples showed protective behaviors in dry and 3% H_2O-containing environments, while in 20% H_2O pre-oxidized samples exhibited sporadic non-protective oxide nodules. The non-protective scales have a similar microstructure from gas-oxide interface to metal-oxide interface: i) Outward grown Fe_3O_4 layer, ii) Inward grown $(Fe,Cr)_3O_4$ spinel layer, and iii) IOZ layer. The protective scales are typically composed of a $(Cr,Mn)_3O_4$ cap layer and a Cr_2O_3 inner layer. As previously reported in numerous studies ([24,28,45], increased humidity deteriorates the protectiveness of chromia scales, even the pre-formed ones, as shown in the present study.

3.3. Effect of surface treatment

Fig. 7a shows the mass gain values of as-received, ground and 800Air-pre-oxidized samples exposed in Ar-5%H_2-3%H_2O. The mass gains clearly showed that the as-received sample had a much greater mass gain (2.6 mg/cm^2) in comparison with ground and pre-oxidized samples, indicating non-protective behavior, as shown in Figs. 2b and 3b. The mass gain values of ground and pre-oxidized samples were identical and very low; thus, protective behavior was observed on ground and pre-oxidized samples (Fig. 7a). Fig. 7b and c illustrate the fuel- and air-side SEM cross-sections of ground samples, respectively. According to Fig. 7b and c, a very thin protective oxide scale of around 33 ± 8 nm on air and 146 ± 21 nm on fuel side was observed on both sides. Additionally, a recrystallization layer with a depth of 1 µm was

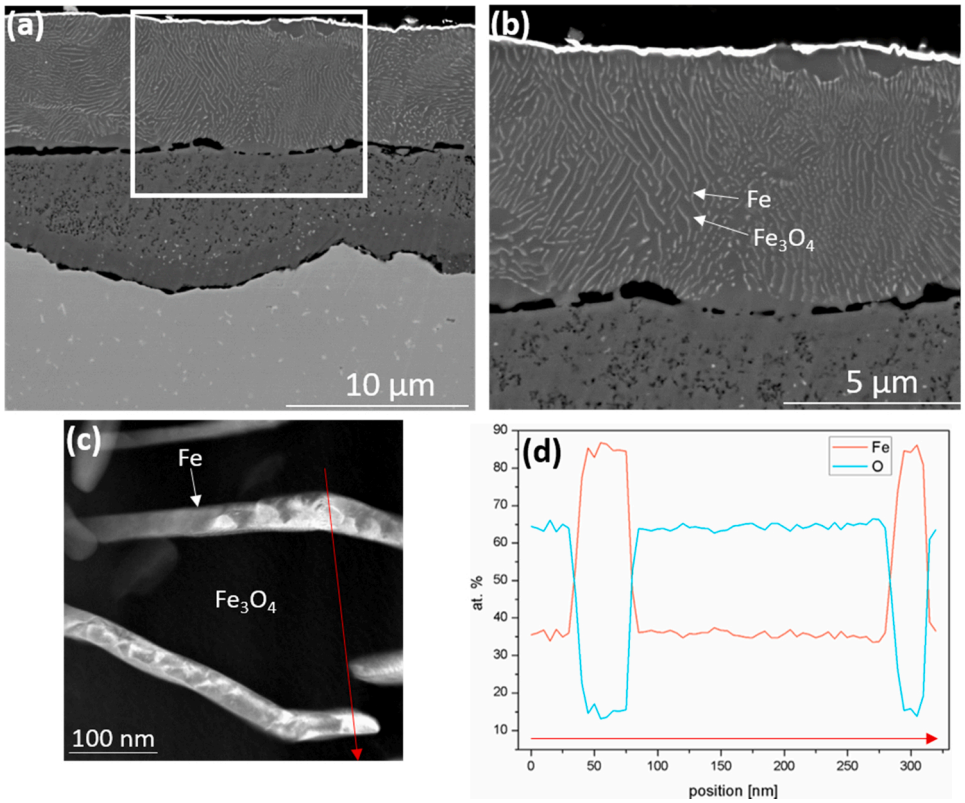

Fig. 4. Cross-sectional SEM images and line TEM-EDX analysis of the lamellar structure on as-received sample exposed at 650 °C in dual atmosphere conditions under Ar-5%H_2-3%H_2O after 336 h. a,b) Cross sectional SEM images, c) TEM image the area where the line scan has performed. D) TEM-EDX line scan data.

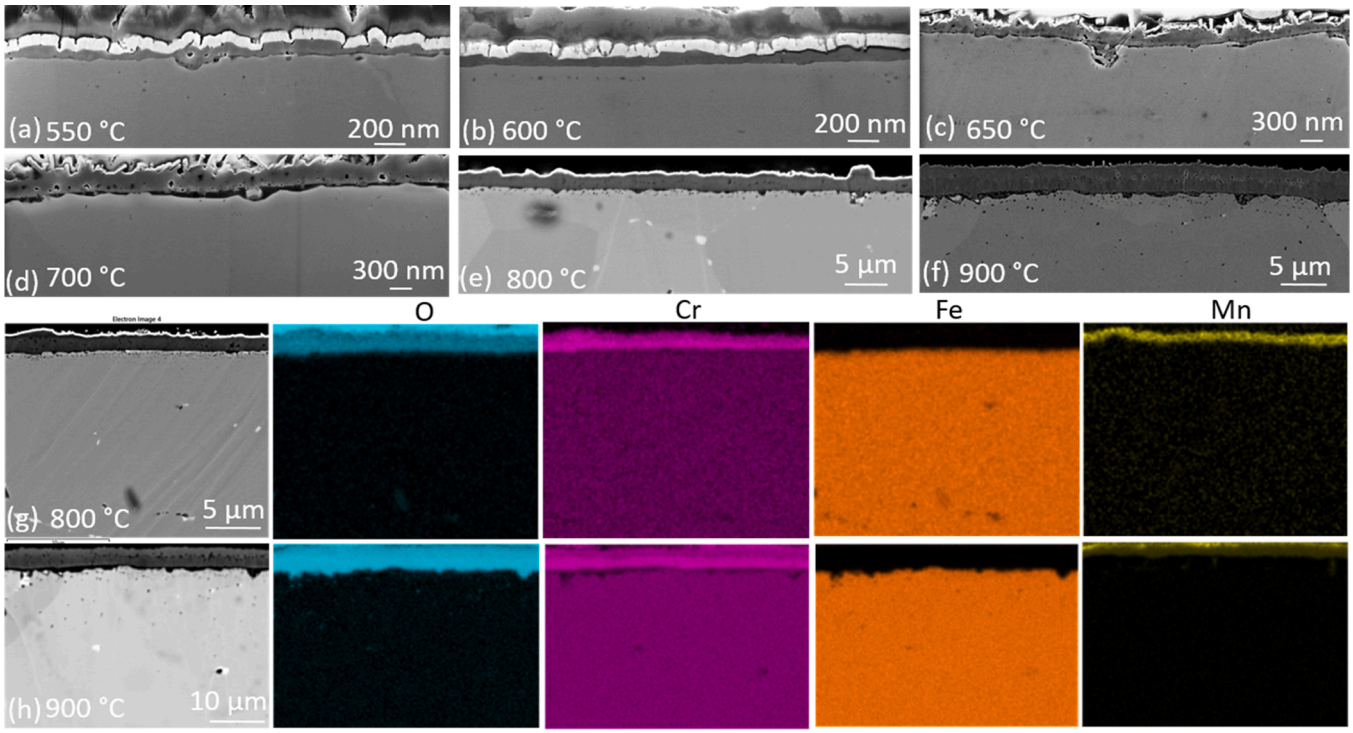

Fig. 5. Cross-sectional SEM images of 800Air-pre-oxidized samples exposed in Ar-5%H_2-3%H_2O between 550 and 900 °C. Except 900 °C analysis was performed on the dual atmosphere exposure samples. Note the different magnifications.

detected below the Cr_2O_3 scale. The average grain size within this layer was approximately 100 nm.

Fig. 8 illustrates the cross-sectional SEM analysis of fuel and the air sides of the as-received samples, exposed between 550 and 800 °C for 336 h in Ar-5%H_2-3%H_2O vs. Air + 3%H_2O. A comparison of the thickness values between fuel and air side is also given in Fig. 8.

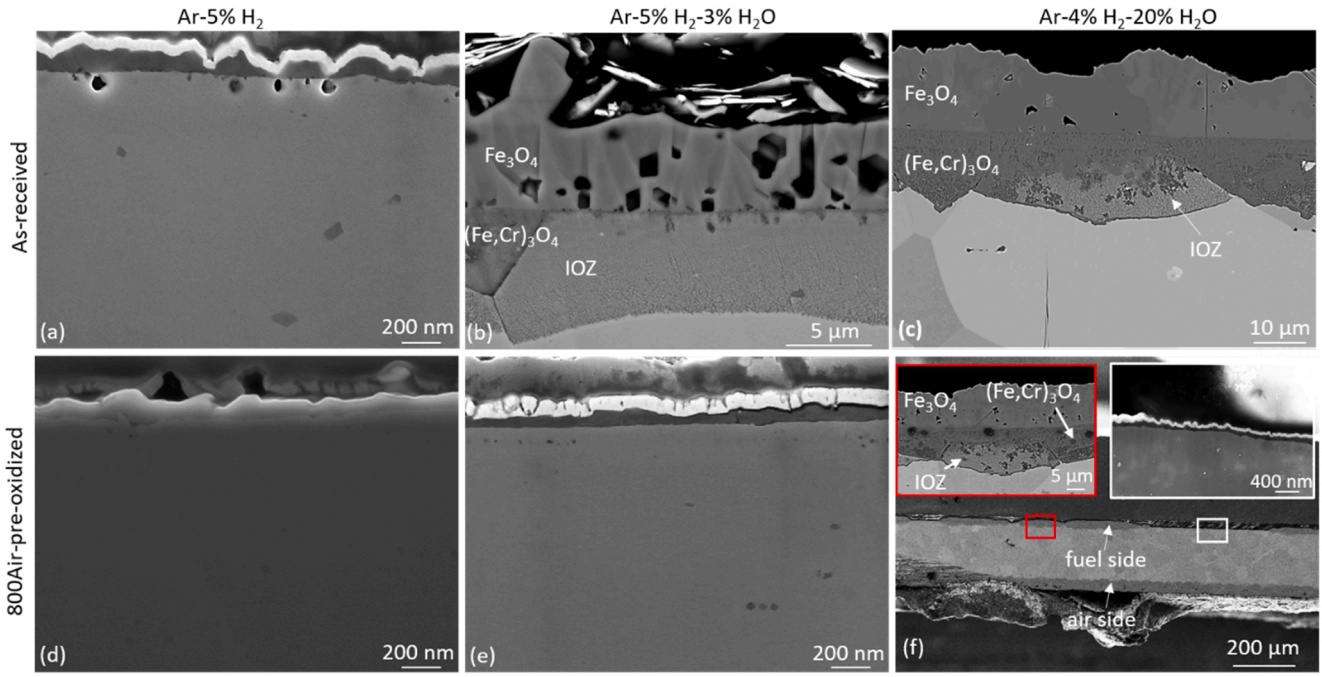

Fig. 6. Fuel side cross-sectional SEM images of as-received and 800Air-pre-oxidized samples exposed at 600 °C for 336 h in dual atmosphere conditions under different fuel utilization. Red and White boxes are representing non-protective and protective regions respectively. Note the different magnifications.

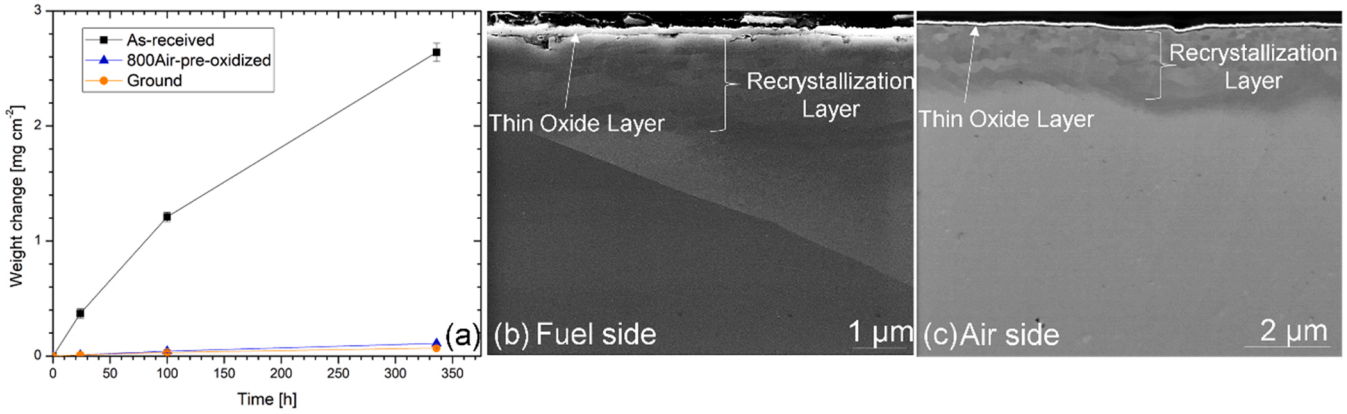

Fig. 7. Mass gains of as-received, 800Air-pre-oxidized and ground samples under single Ar-5%H_2-3%H_2O (a) and Cross-sectional SEM images of fuel (b) and air side (c) of ground non-pre-oxidized samples exposed in dual Ar-5%H_2-3%H_2O and Air+ 3%H_2O atmosphere at 600 °C up to 336 h. Note the different magnifications.

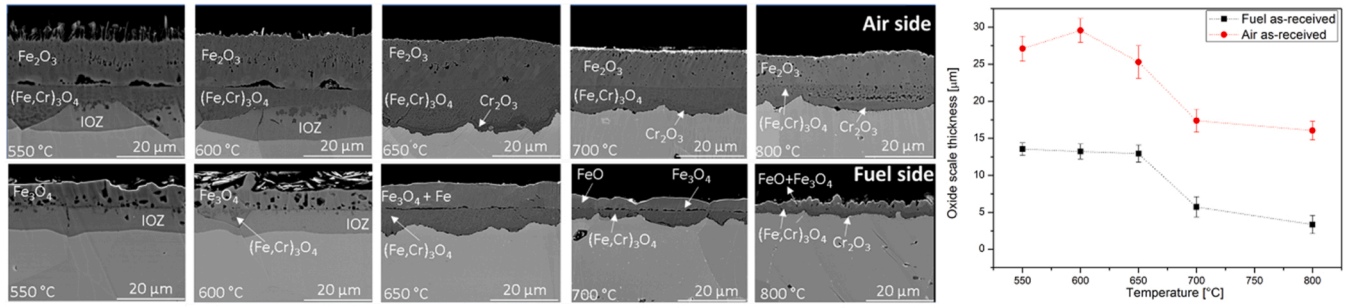

Fig. 8. Comparison of air and fuel sides of as-received samples exposed in Ar-5%H_2-3%H_2O and Air+ 3%H_2O dual atmosphere conditions for 336 h between 550 and 800 °C.

According to the images and the thickness values, it is clear that the non-protective iron oxides on the air side are much thicker compared to ones formed on the fuel side. Furthermore, in both air and fuel sides, the thickness of iron oxide layers decreases as the temperature rises, showing the beneficial effect of temperature.

Fig. 9 depicts the fuel side of the 600Air- and 600H_2-pre-oxidized samples after 336 h of dual-atmosphere exposures at 600 ºC with Ar-5% H_2-3%H_2O on the fuel side. These sample were pre-oxidized for 36 h and 11 h respectively in order to achieve a pre-oxidation scale of the same thickness as 800Air. Fig. 9 clearly showed that 600Air and 600H_2 pre-oxidation procedures resulted in non-protective behavior on the fuel side. These results show that, only 800Air pre-oxidation procedure results in a protective behavior on the fuel side at the entire temperature range (550–800 ºC).

4. Discussion

4.1. Temperature dependence and Cr diffusion

The effect of temperature on the protectiveness of the oxide scale on the air side dual atmosphere conditions was discussed in the previous study on as-received and pre-oxidized AISI 441 steel [33]. Considering that the steel grade 441 is fully protective in air (single atmosphere) at 600–800 ºC [16], the main reason for non-protective Fe-base oxide formation on the air side of the samples exposed in dual-atmosphere conditions is interpreted as the impeded Cr diffusion especially at the grain boundaries in the steel. This interpretation was based on the analysis of the available kinetic data, i.e., oxygen permeability, chromia scaling rate, Cr diffusivity in BCC, and activation energies. Wagner's criteria for internal/external oxidation [46] and maintenance of an already formed external scale [47] were employed to carry out the analysis. For more details, the reader is referred directly to [33].

At 550 and 600 ºC the oxide scales were much more porous compared to the ones formed at 650, 700 and 800 ºC. Formation of more porous outward grown Fe_3O_4 layers at lower temperatures was also observed by Young et al. [27]. At 550 and 600 ºC, below the magnetite layer, the inward grown part consists of an IOZ while at temperatures above 600 °C the IOZ layer was replaced with the $(Fe,Cr)_3O_4$ spinel layer. It is proposed that the formation of a thick inner $(Fe,Cr)_3O_4$ layer slowed down the cation transport toward the surface compared to only an IOZ being present, thus a pore free scale was obtained. It was also shown in previous studies that when this layer contained more Cr it decelerated the growth of the external layer [35].

A comparison of the oxide scales formed at 650 and 700 °C revealed a lamellar structure due to eutectoid decomposition of FeO into $Fe+Fe_3O_4$ was present at 650 °C while no lamellar structure was observed at 700 °C. Instead, a magnetite layer termed as magnetite seam was formed at the FeO-original metal interface. Shizukawa et al. [41], found by exposing Fe-Au alloys that the Au layer formed at the metal-oxide interface and proposed that this layers acts as a barrier against Fe diffusion towards the substrate and promoted eutectoid transformation by enriching the FeO layer. These results suggest that the magnetite seam formation acts in the same way by preventing the diffusion of Fe towards the metal. Yet in the present study, although the magnetite seam layer was present at the metal-oxide interface on the samples exposed at 700 °C the lamellar structure was missing. However, the Fe diffusion rate within the FeO matrix which is a function if iron vacancy concentration also plays a crucial role as showed by Tanei et al. [48]. Tanei showed by high temperature XRD analysis that, the wustite formed at higher temperatures contained less iron vacancies, which resulted in the retardation of eutectoid transformation. Therefore, it is also reasonable to assume that the scale formed at 700 ºC contains more Fe^{+2} ions compared to 650 °C. Thus, cooling with 1 °C/min might not be slow enough for the eutectoid transformation to occur.

An enrichment of the $(Fe,Cr)_3O_4$ layer with Cr at elevated temperatures above 650 °C (Fig. 3.) slowed down both the growth of outward and inward grown layers. Especially above 700 °C, the oxide scales on the as-received specimens gradually transformed into continuous Cr_2O_3

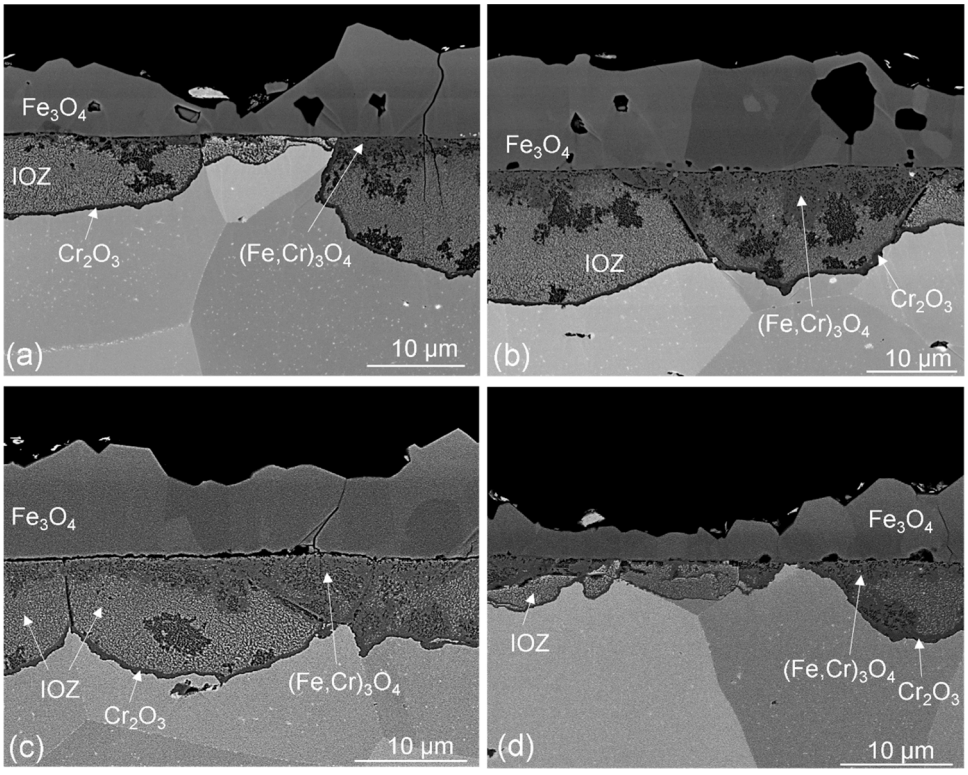

Fig. 9. Fuel side cross-sectional SEM images of 600Air and 600H_2-pre-oxidized samples exposed in dual atmosphere conditions after 336 h at 600 ºC a,b) 600H_2-pre-oxidized sample, c,d) 600Air-pre-oxidized sample.

layer, albeit still overlaid by iron-rich oxides at 800 ºC (Figs. 2e, 3e). At 900 °C, in addition to the whisker-like manganese-rich features at the gas-oxide interface, a typical protective double-layered oxide scale consisting of $(Cr,Mn)_3O_4$ and Cr_2O_3 was obtained. On the other hand, the pre-oxidized specimens exhibited protective scales composed of $(Cr,Mn)_3O_4$ and Cr_2O_3 in the entire temperature range (550–900 °C).

The beneficial effect of temperature was also reflected in the mass gain values. At 800 °C, due to the Fe incorporation to the oxide scale, as-received samples demonstrated a slightly higher mass gain compared to the 800Air-pre-oxidized sample. At 900 °C, both samples showed almost identical mass gains, which indicates that as-received samples are more protective at 900 °C than at 800 ºC. This is a clear result of enhanced bulk Cr transport toward the metal-oxide interface at elevated temperatures (>700 ºC), which promotes protective scaling.

The effect of cold work was also investigated in the present study (Fig. 7a, b). As-received samples showed much higher mass gains (2.5 mg/cm^2) in comparison with the ground and 800Air-pre-oxidized samples, which showed similar mass gains. This indicates that ground and 800Air-pre-oxidized samples showed a protective behavior (Fig. 7a). In Fig. 7b it is clear that, due to the grinding, a recrystallized layer formed just below the original metal surface, which increased the grain boundary density significantly as the average grain size in this layer was approximately 100 nm. In Fig. 7c it was shown that the recrystallization layer is not only beneficial on the fuel side but also improves the protectiveness on the air side. The effect of the grain size of the metal on the protectiveness of Cr_2O_3 scales has also been discussed in the literature and it has been shown that small grain size increases the Cr flux towards the metal-oxide interface, which is beneficial to maintain the presence of an already formed Cr_2O_3 [49]. In contrast, as-received samples were completely covered with Fe-base non-protective oxide as the grain size for annealed AISI 441 is 29 μm. Thus, this effect is an additional indirect proof of the key role of Cr diffusion in the dual-atmosphere/hydrogen effect since as-received AISI 441 is not protective in the as-received condition.

4.2. Effect of water vapor on the oxidation of as-received and 800Air-pre-oxidized samples

Cr_2O_3 scales are known to grow faster in humid and/or hydrogen-containing gases [50–52]. When H_2O is the main oxidant, Cr_2O_3 grows predominantly inward, as demonstrated by O^{18}/O^{16}-tracer experiments [52]. This provides better adherence to the metal [50,53–55] and results in a relatively fine-grained structure [50,56,57]. The effect of water/hydrogen has been argued to be similar to that of reactive elements [58], by H_2O segregating to GBs and thus pinning them, which blocks the grain growth. Yet, according to the studies of Zurek et al. [52] and Niewolak et al. [59], the addition of Mn substantially decreased the mass gain compared to Ni-Cr and Fe-Cr alloys in H_2/H_2O mixtures. In fact, the mass gains were even lower than Mn containing Ni-Cr and Fe-Cr alloys oxidized in air [52,59]. The same trend was also observed by Guillou et al. [60] on alloy 230 which is a Ni-Cr alloy that contains 0.5 wt% Mn. Since, Cr_2O_3 grows mainly inward in H_2/H_2O environments, Niewolak et al. [59] claimed that, the presence of spinel as a continuous cap layer slows down the diffusion of water vapor species such as hydroxides, thus ending up with a slower growth rate on the fuel side.

In the present study water vapor had a detrimental effect on the protectiveness of the as-received and 800air-pre-oxidized samples as shown by the cross-sectional SEM images (Fig. 6). In dry conditions as-received samples formed only Cr_2O_3 scales since the pO_2 at 600 ºC in dry Ar-5%H_2 (1.1×10^{-27} bar) is well below the FeO dissociation pressure (1.3×10^{-25} bar). However, increasing the humidity concentration to 3% resulted in the formation of Fe-rich oxides while further increasing the humidity concentration to 20% H_2O resulted in even thicker Fe-rich non-protective layers. The same effect of water vapor was also observed by Hooshyar et al. [45] at 600 ºC on 304 L resulting in thicker outward grown Fe_3O_4 and inward grown $(Fe,Cr)_3O_4$ layers. Hooshyar et al. [45] showed that, the breakaway oxidation is preceded by the formation of Cr_2O_3. In other words, Cr_2O_3 forms first but cannot be maintained on the surface. The failure of pre-oxidized Cr_2O_3 scales will be discussed in the subsequent section. It should be noted that, when the water vapor concentration increases from 3% to 20%, both pH_2O and pO_2 increases while pH_2 decreases simultaneously. These factors were individually investigated by Hooshyar et al. [45]. The authors concluded that, rather than pO_2 and pH_2, pH_2O is responsible for the failure of the Cr_2O_3 scale in H_2/H_2O mixtures. Yet no explanation was given for the effect of increasing pH_2O. Essuman et al. [24] investigated Fe-10Cr and Fe-20Cr model alloys in Ar-4%H_2-7%H_2O and Ar-7%H_2O between 900 and 1050 ºC and also found that, under low pO_2 environments increasing water vapor concentration resulted in the formation of Fe-rich scales and a drastic increase in mass gains. Essuman et al. [24] claimed that, this trend is correlated with the enhanced internal oxidation of Cr by the expansion of Fe-Cr lattice due to dissolved hydrogen. Dissolved hydrogen in return, increases the oxygen permeation towards the metal thus preventing Cr diffusion towards the surface. However, several studies showed that dissolved hydrogen has no effect on oxygen permeability [61–63]. Thus, it is speculated that Cr_2O_3 fails earlier in 20% water vapor, hence the Fe-rich scales will have grown thicker compared to the 3% H_2O water vapor containing environment. The indication for earlier failure of Cr_2O_3 scale can be found by comparing the progression between inward grown layers: in 3% H_2O, only localized $(Fe,Cr)_3O_4$ formation was observed while in 20% H_2O, more inward grown spinel was present. Yet, time resolved exposures with very short exposure durations are needed to clarify this hypothesis.

The situation of the 800Air-pre-oxidized samples is different. In the present study it was shown that, 800Air-pre-oxidized samples showed protective behavior in Ar-5%H_2-3%H_2O within the investigated temperature range while they partially failed at 600 ºC under Ar-4%H_2-20% H_2O. In the present study, the thickness of the oxide scale in 3%H_2O humidity corresponds to 64 ± 17 nm while under 20% H_2O, in the protective region, the corresponding value is 82 ± 20 nm. These values indicate that, the oxidation rate of the 800Air-pre-oxidized sample in 20% water vapor is slightly higher. That a higher concentration of H_2O increases the scaling rate can also be found by comparing the thickness of as-received sample oxidized in dry Ar-5%H_2 (~900 ppm H_2O) and the ground non-pre-oxidized sample exposed in Ar-5%H_2-3%H_2O. In the former the measured thickness was 97 ± 20 m while on the latter the scale thickness was measured as 146 ± 21 nm. The reason why increased pH_2O increases oxidation rate of Cr_2O_3 both on non-pre-oxidized and 800Air-pre-oxidized samples are unclear at the moment.

4.3. Effect of different pre-oxidation procedures on the protectiveness

Pre-oxidation is a widely used method to protect metallic interconnect materials against high temperature oxidation in SOFC applications [64–68]. The beneficial effect of pre-oxidation in dual atmosphere oxidation was also shown by several authors [16,17,69]. Yet, results obtained by the present study showed that, only 800Air-pre-oxidized samples were protective in Ar-5%H_2-3%H_2O as shown by mass gains and thickness values (Fig. 1.) and microscopy (Fig. 5). On the contrary, the as-received samples (Fig. 2.) and 600Air and 600H_2-pre-oxidized samples (Fig. 9) failed in the same environment at 600 °C. This is an important outcome since it was previously mentioned in the effect of water vapor section that as-received samples form a Cr_2O_3 layer first and fail afterwards. Thus, as-received samples fail similarly to samples pre-oxidized at 600 °C showing that the Cr_2O_3 scale that forms at 600 °C cannot be maintained. Hence, although the layer thickness values are identical for each pre-oxidation procedure, they do not show the same oxidation behavior indicating that other properties of these pre-formed layers determine its protectiveness. According to previous studies the following differences are expected:

1) It is expected that pre-oxidation at higher temperatures (800Air-pre-oxidation) will result in rather coarse-grained Cr_2O_3 scales [70] hence, lower growth rates at 600 °C. At the same time, Cr_2O_3 pre-grown at 600°C and in particular in H_2/H_2O is expected to demonstrate faster scaling rates and worse protectiveness owing to the preformed fine-grained Cr_2O_3 scale. It has been shown in numerous studies that below 800 °C, grain boundary transport in oxide scales dominates the oxidation process [71,72], making the scaling rate sensitive to the Cr_2O_3 grain size. Another important factor affecting the grain size is the temperature. Sabioni et al. [70] studied the oxidation of Fe-15Cr model alloys in air and reported an average grain size of 400 nm at 750 °C and 700 nm at 900 °C. Hallström et al. [73] exposed pure chromium in O_2 for 24 h at 650 °C and observed 100 nm wide columnar Cr_2O_3 grains in the inner part of the scale while the outer layer consisted of 200 nm wide grains. The 100 nm wide grains were also obtained by Bataillou et al. [72] in the Cr_2O_3 grown after 50 h exposure at 700 °C in impure argon. Therefore, the chromia grain size is expected to decrease in the order of 800Air, 600Air, 600H_2.
2) Spinel coverage differs depending on pre-oxidation and affect the scaling rate. Niewolak et al. [59] found that a cap layer of $(Cr,Mn)_3O_4$ forms substantially faster in air compared to H_2/H_2O. Furthermore, the authors observed a decrease in oxidation rate that is attributed to complete spinel coverage. In the present case it is thus reasonable to assume that 800Air pre-oxidation results in the most complete spinel coverage, followed by 600Air. The sample with least spinel coverage is expected to be 600H_2.
3) It has been shown earlier that Cr_2O_3 scales formed at lower temperature incorporated more Fe than scale formed at higher temperature [74]. Although this could explain the difference in protectiveness between 800Air and 600Air this hypothesis fails for the 600H_2 samples. These samples were pre-oxidized in Ar-5–0.3% H_2O where Fe oxide formation is not possible, thus these scales are expected to be Fe free. Consequently, further characterization of these pre-formed layers by advanced techniques such as TEM is needed to reveal the grain-size, texture and phase constituents.

4.4. Comparison of air and fuel sides of the samples after exposure

The most striking experimental observation in this study is the differences on the intensity of corrosion between fuel and air sides [33]. When the samples are exposed in the as-received condition, the oxide scales on the air side are at least twice as thick as those on the fuel side (Fig. 8). It is established above that Cr_2O_3 grows faster in H_2/H_2O than in air, the opposite behavior is observed here. The reason for this discrepancy is that after the failure of the Cr_2O_3 scales, Fe-rich non-protective oxides grow on both sides of the specimen. Oxidation of pure iron in air and Ar/H_2O or H_2/H_2O have been investigated in several studies [75–77]. According to Caplan et al. [75], pure iron oxidizes more slowly in Ar/H_2O mixture than in air at 550 °C. Furthermore, Turkdogan et al. [76] studied the effect of pH_2O in H_2/H_2O mixtures on the growth of FeO layers and found a similar result. Additionally, Galerie et al. [77] also stated that, metal deficient p-type oxides such as NiO or FeO oxidize slowly in low pO_2 environments as the concentration of the metal vacancies are pO_2 dependent and are higher in high pO_2 environments. In addition to NiO and FeO, a study revealed that, Fe_2O_3 shows p-type semiconductor behavior in high pO_2 environments and the pO_2 dependency was equilibrated as: $[V'''_{Fe}] \approx (pO_2)^{3/16}$ [78]. Furthermore, magnetite was also shown to be cation deficient and the deficiency increases at higher oxygen potentials [79]. Therefore, it is reasonable for Fe-rich oxides to grow faster in air compared to low pO_2 H_2/H_2O environment.

The second observation is the different protectiveness of the pre-grown chromia scale (800Air-pre-oxidation) on the air and fuel sides (50 nm). The chromia pre-grown at 800 °C for 20 min remained stable and protective on the fuel side (Fig. 1, Fig. 5) throughout the entire temperature range, while it failed on the air side at 550–700 °C after 336 h [33]. Alnegren et al. [16] investigated samples that were pre-oxidized for 3 h at 800 °C. While the fuel side of these samples remained protective, they failed on the air side within 1000 h at 600 °C. However, it should be noted this occurs only under dual atmosphere conditions, the samples are entirely protective in single atmosphere air exposure. Therefore, both studies confirm that samples pre-oxidized at 800 °C in air are more protective on the fuel side than on the air side under dual atmosphere conditions. In normal circumstances, one would expect that the fuel side should be more corrosive owing to the presence of water vapor, since Cr_2O_3 scales grow faster in H_2/H_2O mixtures, as discussed previously. On the air side, the growth rate should be slow and protective. When compared, these atmospheres differ from each other in terms of oxygen potential. It can be speculated that increasing pO_2 might result in higher oxidation rates of Cr_2O_3 scales. However, the growth rates of Cr_2O_3 scales are shown to be independent of oxygen partial pressure at 1000 °C between 10^{-13} and 10^{-3} atm on Ni-30Cr model alloys [80]. It can be also speculated that the presence of H increases the growth rate of Cr_2O_3 scales. However, according to the results of Alnegren et al. [16], under dual-atmosphere conditions, on pre-oxidized samples (800 °C, 3 h), the growth rates of Cr-rich thin oxide scales on the air side in the presence of dissolved hydrogen in the metal are approximately equal to the formed in single atmosphere. Therefore, the presence of dissolved hydrogen in the metal does not increase the growth rate of Cr_2O_3 scales on the air side. The reason for failure on the air side is explained by the deceleration of Cr diffusion [33], since ground non-pre-oxidized samples were protective on the air side under the same oxidation conditions (Fig. 7c). However, as hydrogen diffuses from the fuel to the air side of the specimens the concentration of hydrogen should be higher on the fuel side than on the air side. Thus, any effects related to the presence of hydrogen, such as the deceleration of Cr transport to the surface, should lead to failure on the fuel side as well. Whether the samples fail or not is governed by the interplay between Cr consumption and supply. In general, if Cr consumption exceeds Cr supply, Cr_2O_3 cannot be sustained. In the present study, as-received samples and even 800Air-pre-oxidized samples failed on the air side while ground samples were protective on both the air and fuel sides due to enhanced Cr transport toward the surface. This illustrates that increased Cr transport due to the fine-grained recrystallization zone was sufficient to maintain the protective Cr_2O_3 scale. Thus, it can be speculated that the failure of pre-oxidized samples on the air side in dual-atmosphere conditions can be related to an additional mechanism that affects the Cr consumption. One conceivable mechanism is Cr evaporation, which depletes the Cr supply of the material and is absent on the fuel side. Alnegren et al. [16] performed dual-atmosphere exposures in dry air and still observed Fe-rich oxide formation, although the intensity of the corrosion was less in dry conditions. Further dedicated experiments are needed to verify and/or quantify the effect of hydrogen on Cr transport in ferritic steels, establish the nature of this effect (GB or lattice diffusion), and develop appropriate mitigation strategies.

5. Conclusion

The steel grade AISI 441 demonstrated poor performance in a simulated SOFC fuel gas Ar-H_2-H_2O in comparison with air (single atmosphere). In H_2/H_2O, the exposure parameters such as temperature, surface condition and humidity had the following effect on the oxide scale protectiveness:

- As received samples exposed at 550–700 °C, exhibited breakaway-type oxide scales composed of external Fe-rich oxides and internally grown $(Fe,Cr)_xO_y$-rich IOZ or continuous sublayers.
- Pre-formed chromia layers (50 nm) generally improve the performance of AISI441 in Ar-H_2-H_2O. However, the pre-oxidation

conditions play a key role in the protectiveness of the pre-grown oxide layer.

- The scales pre-formed at 600 ºC demonstrated substantially lower protectiveness in comparison with those grown at 800 ºC.
- Increased humidity breaks down the most protective chromia scale type (800Air), leading to the formation of Fe-rich nodules in Ar-5% H_2-20%H_2O at 600 ºC while the same chromia scale demonstrated full protectiveness in Ar-5%H_2-3%H_2O. Higher humidity is believed to accelerate the chromia scaling rate.
- The breakdown of the oxide scale on the air side in dual-atmosphere conditions occurs because hydrogen impedes Cr diffusion. This effect should be at least equally strong on the H_2/H_2O side, yet a pre-oxidized scale (800Air) remains protective. The reason for this discrepancy is presently unknown.
- Future work such as on model Fe-Cr and Fe-Cr-Mn alloys are needed to deconvolute the effect of grain size and spinel coverage on the protectiveness of 800Air-pre-oxidized specimens.
- The results show that fuel side oxidation of the interconnect can cause severe degradation, in particular at IT-SOFC temperatures. The results suggest that a short high temperature pre-oxidation or stack conditioning step can reduce the degradation.

CRediT authorship contribution statement

Anton Chyrkin: Conceptualization, Investigation, Writing – original draft, Writing – review & editing. **Kerem Ozgur Gunduz:** Conceptualization, Investigation, Writing – original draft, Writing – review & editing. **Jan-Erik Svensson**: Funding Acquisition, Project Administration, Supervision. **Jan Froitzheim:** Conceptualization, Funding Acquisition, Project Administration, Supervision, Writing – review & editing.

Declaration of Competing Interest

The authors declare that they have no known competing financial interests or personal relationships that could have appeared to influence the work reported in this paper.

Data Availability

The raw/processed data required to reproduce these findings will be made available on request.

Acknowledgements

The authors gratefully acknowledge Swedish Energy Agency (Grant: 2015-009652), The FFI program as well as the Swedish High Temperature Corrosion Centre for providing funding for this study. Microstructural Investigations were carried out at the Chalmers Material Analysis Laboratory, CMAL. One of the Authors of this work, Kerem Ozgur Gunduz acknowledges financial support of Scientific and Technological Research Council of Turkey through the program number TUBITAK-2219.

References

[1] R.P. O'hayre, Fuel Cell Fundamentals, John Wiley & Sons, Hoboken, N.J, 2006.
[2] K. Kendall, M. Kendall, High-Temperature Solid Oxide Fuel Cells for the 21st Century: Fundamentals, Design and Applications, Academic Press is an imprint of Elsevier, London, 2016, pp. 1 online resource (xii, 508 pages).
[3] E.D. Wachsman, C.A. Marlowe, K.T. Lee, Role of solid oxide fuel cells in a balanced energy strategy, Energ. Environ. Sci. 5 (2012) 5498–5509.
[4] Elcogen OY. Solid Oxide Fuel Cells: Opportunities for a clean energy future, 2019. ⟨https://elcogen.com/wp-content/uploads/2019/04/elcogen-sofc-white-paper-2019.pdf⟩, in.
[5] J.A. Kilner, M. Burriel, Materials for intermediate-temperature solid-oxide fuel cells, Annu Rev. Mater. Res 44 (2014) 365–393.
[6] J.W. Fergus, Metallic interconnects for solid oxide fuel cells, Mat. Sci. Eng. a-Struct. 397 (2005) 271–283.
[7] J.C.W. Mah, A. Muchtar, M.R. Somalu, M.J. Ghazali, Metallic interconnects for solid oxide fuel cell: a review on protective coating and deposition techniques, Int J. Hydrog. Energ. 42 (2017) 9219–9229.
[8] J.W. Wu, X.B. Liu, Recent development of SOFC metallic interconnect, J. Mater. Sci. Technol. 26 (2010) 293–305.
[9] W.Z. Zhu, S.C. Deevi, Development of interconnect materials for solid oxide fuel cells, Mat. Sci. Eng. a-Struct. 348 (2003) 227–243.
[10] D.J.L. Brett, A. Atkinson, N.P. Brandon, S.J. Skinner, Intermediate temperature solid oxide fuel cells, Chem. Soc. Rev. 37 (2008) 1568–1578.
[11] J. Froitzheim, E. Larsson, L.G. Johansson, J.E. Svensson, Cr evaporation of metallic interconnects: a novel method for quantification, solid oxide, Fuel Cells 11 (Sofc-Xi) 25 (2009) 1423–1428.
[12] J. Froitzheim, H. Ravash, E. Larsson, L.G. Johansson, J.E. Svensson, Investigation of chromium volatilization from FeCr interconnects by a denuder technique, J. Electrochem Soc. 157 (2010) B1295–B1300.
[13] H. Falk-Windisch, J.E. Svensson, J. Froitzheim, The effect of temperature on chromium vaporization and oxide scale growth on interconnect steels for Solid Oxide Fuel Cells, J. Power Sources 287 (2015) 25–35.
[14] C. Goebel, A.G. Fefekos, J.E. Svensson, J. Froitzheim, Does the conductivity of interconnect coatings matter for solid oxide fuel cell applications? J. Power Sources 383 (2018) 110–114.
[15] P. Alnegren, M. Sattari, J.E. Svensson, J. Froitzheim, Severe dual atmosphere effect at 600 degrees C for stainless steel 441, J. Power Sources 301 (2016) 170–178.
[16] P. Alnegren, M. Sattari, J.E. Svensson, J. Froitzheim, Temperature dependence of corrosion of ferritic stainless steel in dual atmosphere at 600-800 degrees C, J. Power Sources 392 (2018) 129–138.
[17] C. Goebel, P. Alnegren, R. Faust, J.E. Svensson, J. Froitzheim, The effect of pre-oxidation parameters on the corrosion behavior of AISI 441 in dual atmosphere, Int. J. Hydrog. Energ. 43 (2018) 14665–14674.
[18] H. Falk-Windisch, J. Claquesin, J.E. Svensson, J. Froitzheim, The effect of metallic Co-coating thickness on ferritic stainless steels intended for use as interconnect material in intermediate temperature solid oxide fuel cells, Oxid. Met. 89 (2018) 233–250.
[19] H. Falk-Windisch, J. Claquesin, M. Sattari, J.E. Svensson, J. Froitzheim, Co- and Ce/Co-coated ferritic stainless steel as interconnect material for intermediate temperature solid oxide fuel cells, J. Power Sources 343 (2017) 1–10.
[20] H. Falk-Windisch, M. Sattari, J.E. Svensson, J. Froitzheim, Chromium vaporization from mechanically deformed pre-coated interconnects in solid oxide fuel cells, J. Power Sources 297 (2015) 217–223.
[21] Z.G. Yang, M.S. Walker, P. Singh, J.W. Stevenson, Anomalous corrosion behavior of stainless steels under SOFC interconnect exposure conditions, Electrochem. Solid St 6 (2003) B35–B37.
[22] Z.G. Yang, G.G. Xia, M.S. Walker, C.M. Wang, J.W. Stevenson, P. Singh, High temperature oxidation/corrosion behavior of metals and alloys under a hydrogen gradient, Int J. Hydrog. Energ. 32 (2007) 3770–3777.
[23] J. Rufner, P. Gannon, P. White, M. Deibert, S. Teintze, R. Smith, H. Chen, Oxidation behavior of stainless steel 430 and 441 at 800 degrees C in single (air/air) and dual atmosphere (air/hydrogen) exposures, Int. J. Hydrog. Energ. 33 (2008) 1392–1398.
[24] E. Essuman, G.H. Meier, J. Zurek, M. Hansel, W.J. Quadakkers, The effect of water vapor on selective oxidation of Fe-Cr alloys, Oxid. Met. 69 (2008) 143–162.
[25] J. Ehlers, D.J. Young, E.J. Smaardijk, A.K. Tyagi, H.J. Penkalla, L. Singheiser, W. J. Quadakkers, Enhanced oxidation of the 9%Cr steel P91 in water vapour containing environments, Corros. Sci. 48 (2006) 3428–3454.
[26] E. Essuman, G.H. Meier, J. Zurek, M. Hansel, L. Singheiser, W.J. Quadakkers, Enhanced internal oxidation as trigger for breakaway oxidation of Fe-Cr alloys in gases containing water vapor, Scr. Mater. 57 (2007) 845–848.
[27] D.J. Young, J. Zurek, L. Singheiser, W.J. Quadakkers, Temperature dependence of oxide scale formation on high-Cr ferritic steels in Ar-H_2-H_2O, Corros. Sci. 53 (2011) 2131–2141.
[28] J. Zurek, G.H. Meier, E. Wessel, L. Singheiser, W.J. Quadakkers, Temperature and gas composition dependence of internal oxidation kinetics of an Fe-10%Cr alloy in water vapour containing environments, Mater. Corros. 62 (2011) 504–513.
[29] L. Mikkelsen, S. Linderoth, High temperature oxidation of Fe-Cr alloy in O_2-H_2-H_2O atmospheres; microstructure and kinetics, Mat. Sci. Eng. a-Struct. 361 (2003) 198–212.
[30] C.T. Fujii, R.A. Meussner, The mechanism of the high-temperature oxidation of iron-chromium alloys in water vapor, J. Electrochem Soc. 111 (1964) 1215–1221.
[31] A. Galerie, S. Henry, Y. Wouters, M. Mermoux, J.P. Petit, L. Antoni, Mechanisms of chromia scale failure during the course of 15-18Cr ferritic stainless steel oxidation in water vapour, Mater. High. Temp. 22 (2005) 105–112.
[32] W.J. Quadakkers, J. Zurek, M. Hansel, Effect of water vapor on high-temperature oxidation of FeCr alloys, Jom-Us 61 (2009) 44–50.
[33] K.O. Gunduz, A. Chyrkin, C. Goebel, L. Hansen, O. Hjorth, J.E. Svensson, J. Froitzheim, The effect of hydrogen on the breakdown of the protective oxide scale in solid oxide fuel cell interconnects, Corros. Sci. 179 (2021).
[34] P. Piccardo, S. Anelli, V. Bongiorno, R. Spotorno, L. Repetto, P. Girardon, K44M ferritic stainless steel as possible interconnect material for SOFC stack operating at 600 degrees C: characterization of the oxidation behaviour at early working stages, Int J. Hydrog. Energ. 40 (2015) 3726–3738.
[35] B. Pujilaksono, T. Jonsson, H. Heidari, M. Halvarsson, J.E. Svensson, L. G. Johansson, Oxidation of binary FeCr alloys (Fe-2.25Cr, Fe-10Cr, Fe-18Cr and Fe-25Cr) in O_2 and in O_2 + H_2O environment at 600 °C, Oxid. Met. 75 (2011) 183–207.

[36] T. Jonsson, B. Pujilaksono, H. Heidari, F. Liu, J.E. Svensson, M. Halvarsson, L. G. Johansson, Oxidation of Fe–10Cr in O_2 and in O2+H_2O environment at 600 °C: a microstructural investigation, Corros. Sci. 75 (2013) 326–336.

[37] T. Jonsson, S. Karlsson, H. Hooshyar, M. Sattari, J. Liske, J.E. Svensson, L. G. Johansson, Oxidation after breakdown of the chromium-rich scale on stainless steels at high temperature: internal oxidation, Oxid. Met. 85 (2016) 509–536.

[38] Z.F. Li, G.M. Cao, F. Lin, C.Y. Cui, H. Wang, Z.Y. Liu, Phase transformation behavior of oxide scale on plain carbon steel containing 0.4 wt% Cr during continuous cooling, ISIJ Int. 58 (2018) 2338–2347.

[39] S. Hayashi, K. Mizumoto, S. Yoneda, Y. Kondo, H. Tanei, S. Ukai, The mechanism of phase transformation in thermally-grown FeO scale formed on pure-fe in air, Oxid. Met. 81 (2014) 357–371.

[40] S. Hayashi, S. Yoneda, Y. Kondo, H. Tanei, Phase transformation of thermally grown FeO formed on high-purity fe at low oxygen potential, Oxid. Met. 94 (2020) 81–93.

[41] Y. Shizukawa, S. Hayashi, S. Yoneda, Y. Kondo, H. Tanei, S. Ukai, Mechanism of magnetite seam formation and its role for FeO scale transformation, Oxid. Met. 86 (2016) 315–326.

[42] B. Gleeson, S.M.M. Hadavi, D.J. Young, Isothermal transformation behavior of thermally-grown wustite, Mater. High. Temp. 17 (2000) 311–318.

[43] S. Yoneda, S. Hayashi, Y. Kondo, H. Tanei, S. Ukai, Effect of Mn on isothermal transformation of thermally grown FeO Scale Formed on Fe-Mn Alloys, Oxid. Met. 87 (2017) 125–138.

[44] M.R. Ardigo, I. Popa, S. Chevalier, S. Weber, O. Heintz, M. Vilasi, Effect of water vapor on the oxidation mechanisms of a commercial stainless steel for interconnect application in high temperature water vapor electrolysis, Oxid. Met. 79 (2013) 495–505.

[45] H. Hooshyar, T. Jonsson, J. Hall, J.E. Svensson, L. Johansson, J. Liske, The Effect of H_2 and H_2O on the oxidation of 304l-stainless steel at 600 °C: general behaviour (Part I), Oxid. Met. 85 (2016) 321–342.

[46] C. Wagner, Reaktionstypen bei der oxydation von legierungen, Zeitschrift für Elektrochemie, Ber. der Bunsenges. für Phys. Chem. 63 (1959) 772–782.

[47] C. Wagner, Theoretical analysis of the diffusion processes determining the oxidation rate of alloys, J. Electrochem Soc. 99 (1952) 369.

[48] H. Tanei, Y. Kondo, Phase transformation of oxide scale and its control, in: Nippon Steel & Sumitomo Metal Technical Report 2016, pp. 87–91.

[49] C. Ostwald, H.J. Grabke, Initial oxidation and chromium diffusion. I. Effects of surface working on 9-20% Cr steels, Corros. Sci. 46 (2004) 1113–1127.

[50] M. Michalik, M. Hansel, J. Zurek, L. Singheiser, W.J. Quadakkers, Effect of water vapour on growth and adherence of chromia scales formed on Cr in high and low PO_2-environments at 1000 and 1050 degrees C, Mater. High. Temp. 22 (2005) 213–221.

[51] D.J. Young, Effects of water vapour on the oxidation of chromia formers, Mater. Sci. Forum 595–598 (2008) 1189–1197.

[52] J. Zurek, D.J. Young, E. Essuman, M. Hansel, H.J. Penkalla, L. Niewolak, W. J. Quadakkers, Growth and adherence of chromia based surface scales on Ni-base alloys in high- and low-pO_2 gases, Mat. Sci. Eng. a-Struct. 477 (2008) 259–270.

[53] G. Hultquist, B. Tveten, E. Hornlund, Hydrogen in chromium: influence on the high-temperature oxidation kinetics in H_2O oxide-growth mechanisms and scale adherence, Oxid. Met. 54 (2000) 1–10.

[54] B. Tveten, G. Hultquist, T. Norby, Hydrogen in chromium: influence on the high-temperature oxidation kinetics in O_2 oxide-growth mechanisms and scale adherence, Oxid. Met. 51 (1999) 221–233.

[55] A. Galerie, J.P. Petit, Y. Wouters, J. Mougin, A. Srisrual, P.Y. Hou, Water vapour effects on the oxidation of chromia-forming alloys, Mater. Sci. Forum 696 (2011) 200–205.

[56] D. Simon, B. Gorr, M. Hansel, V. Shemet, H.J. Christ, W.J. Quadakkers, Effect of in-situ gas changes on thermally grown chromia scales formed on Ni-25Cr alloy at 1000 °C in atmospheres with and without water vapour, Mater. High. Temp. 32 (2015) 238–247.

[57] M. Hansel, E. Turan, V. Shemet, D. Gruner, U. Breuer, D. Simon, B. Gorr, H. J. Christ, W.J. Quadakkers, Effect of specimen thickness on chromia scaling of Ni25Cr in N_2-O_2-H_2O test gases at 1000 °C, Mater. High. Temp. 32 (2015) 160–166.

[58] S. Chevalier, What did we learn on the reactive element effect in chromia scale since Pfeil's patent? Mater. Corros. 65 (2014) 109–115.

[59] L. Niewolak, D.J. Young, H. Hattendorf, L. Singheiser, W.J. Quadakkers, Mechanisms of oxide scale formation on ferritic interconnect steel in simulated low and high pO_2 service environments of solid oxide fuel cells, Oxid. Met. 82 (2014) 123–143.

[60] S. Guillou, C. Desgranges, S. Chevalier, Study of the growth mechanism of some oxide scales on alloy 230 in high temperature vapor electrolysis (HTVE) conditions, Defect Diffus. Forum 323–325 (2012) 577–582.

[61] A. Prillieux, D. Jullian, J.Q. Zhang, D. Monceau, D.J. Young, Internal oxidation in dry and wet conditions for oxygen permeability of Fe-Ni alloys at 1150 and 1100 °C, Oxid. Met 87 (2017) 273–283.

[62] P.Y. Guo, J.Q. Zhang, D.J. Young, C.H. Konrad, Oxygen permeability measurements in Ni Using H_2/H_2O, CO/CO_2 and Ni/NiO rhines pack atmospheres, Oxid. Met. 83 (2015) 223–235.

[63] A. Chyrkin, C. Cossu, J.-E. Svensson, J. Froitzheim, Effect of hydrogen on the internal oxidation of a Pd-Cr alloy in Dual-Atmosphere conditions, Oxid. Met. (2022).

[64] B. Talic, S. Molin, P.V. Hendriksen, H.L. Lein, Effect of pre-oxidation on the oxidation resistance of Crofer 22 APU, Corros. Sci. 138 (2018) 189–199.

[65] Y.S. Chou, J.W. Stevenson, P. Singh, Effect of pre-oxidation and environmental aging on the seal strength of a novel high-temperature solid oxide fuel cell (SOFC) sealing glass with metallic interconnect, J. Power Sources 184 (2008) 238–244.

[66] S. Fontana, M. Vuksa, S. Chevalier, G. Caboche, P. Piccardo, On the effect of surface treatment to improve oxidation resistance and conductivity of metallic interconnects for SOFC in operating conditions, Mater. Sci. Forum 595–598 (2008) 753–762.

[67] N.J. Magdefrau, L. Chen, E.Y. Sun, M. Aindow, Effects of alloy heat treatment on oxidation kinetics and scale morphology for Crofer 22 APU, J. Power Sources 241 (2013) 756–767.

[68] S.P. Simner, M.D. Anderson, G.G. Xia, Z. Yang, L.R. Pederson, J.W. Stevenson, SOFC performance with Fe-Cr-Mn alloy interconnect, J. Electrochem Soc. 152 (2005) A740–A745.

[69] R. Amendola, P. Gannon, B. Ellingwood, K. Hoyt, P. Piccardo, P. Genocchio, Oxidation behavior of coated and preoxidized ferritic steel in single and dual atmosphere exposures at 800 degrees C, Surf. Coat. Tech. 206 (2012) 2173–2180.

[70] A.C.S. Sabioni, J.N.V. Souza, V. Ji, F. Jomard, V.B. Trindade, J.F. Carneiro, Study of ion diffusion in oxidation films grown on a model Fe-15%Cr alloy, Solid State Ion. 276 (2015) 1–8.

[71] D. Caplan, G.I. Sproule, Effect of oxide grain structure on high-temperature oxidation of Cr, Oxid. Met. 9 (1975) 459–472.

[72] L. Bataillou, L. Martinelli, C. Desgranges, S. Bosonnet, K. Ginestar, F. Miserque, Y. Wouters, L. Latu-Romain, A. Pugliara, A. Proietti, D. Monceau, Growth kinetics and characterization of chromia scales formed on Ni-30Cr alloy in impure argon at 700 oC, Oxid. Met. 93 (2020) 329–353.

[73] S. Hallstrom, M. Halvarsson, L. Hoglund, T. Jonsson, J. Agren, High temperature oxidation of chromium: kinetic modeling and microstructural investigation, Solid State Ion. 240 (2013) 41–50.

[74] K. Segerdahl, J.E. Svensson, L.G. Johansson, Protective and nonprotective behavior of 11% Cr steel in O_2+H_2O environment at 450-700 oC, J. Electrochem Soc. 151 (2004) B394–B398.

[75] D. Caplan, M. Cohen, Effect of cold work on the oxidation of iron in water vapour at 550 °C, Corros. Sci. 7 (1967) 725–727.

[76] E.T. Turkdogan, W.M. Mckewan, L. Zwell, Rate of oxidation of iron to wustite in water-hydrogen gas mixtures, J. Phys. Chem. 69 (1965) 327–334.

[77] A. Galerie, Y. Wouters, M. Caillet, The kinetic behaviour of metals in water vapour at high temperatures: can general rules be proposed? Mater. Sci. Forum (2001) 231–238.

[78] J. Wang, N.H. Perry, L.J. Guo, L. Vayssieres, H.L. Tuller, On the theoretical and experimental control of defect chemistry and electrical and photoelectrochemical properties of hematite nanostructures, ACS Appl. Mater. Int. 11 (2019) 2031–2041.

[79] R. Dieckmann, H. Schmalzried, Defects and cation diffusion in magnetite.6. point-defect relaxation and correlation in cation tracer diffusion, Ber. Bunsen Phys. Chem. 90 (1986) 564–575.

[80] E. Schmucker, C. Petitjean, L. Martinelli, P.J. Panteix, S. Ben Lagha, M. Vilasi, Oxidation of Ni-Cr alloy at intermediate oxygen pressures. I. Diffusion mechanisms through the oxide layer, Corros. Sci. 111 (2016) 474–485.